Structurally stitched NCF preforms: Quasi-static response

V. Koissin [a,1], J. Kustermans [a,2], S.V. Lomov [a,*], I. Verpoest [a], B. Van Den Broucke [a,b], V. Witzel [c]

[a] Dept. of Metallurgy and Materials Engineering, Katholieke Universiteit Leuven, Kasteelpark Arenberg 44, B-3001 Heverlee, Belgium
[b] EADS Innovation Works, D-81663 Munich, Germany
[c] Inst für Flugzeugbau, Universität Stuttgart, Pfaffenwaldring 31, D-70569 Stuttgart, Germany

ARTICLE INFO

ABSTRACT

Experimental data are presented for a typical structurally stitched preform, composed of carbon fibre non-crimp fabrics (NCFs) and impregnated with an epoxy resin. The term 'structural' presumes here that the stitching yarn does not only consolidate the layers (as the non-structural one does for NCF plies) but forms also a through-the-thickness reinforcement. One stitching technique—tufting—is studied, with 67 tex carbon yarn and several stitching lengths. The test results (in-plane tension, out-plane compression, and 3-point bending) are compared and discussed revealing an influence of stitching and specifics of damage development. The stitching, on the one hand, decreases delaminations and increases the ultimate load. On the other hand, the stitching creates stress–strain concentrators which lead to earlier damage initiation.

© 2009 Elsevier Ltd. All rights reserved.

1. Introduction

Structural (i.e. with a relatively thick and strong yarn) stitching is often used to make easier the lay-up process and to improve the delamination resistance as well as the out-of-plane stiffness of a textile composite. On the other hand, these advantages are accompanied by a significant distortion of the initial fabric structure by the needle movement and inserted yarn: fibre-free zones ("openings"), breakage and vertical movement (crimpling) of fibre tows, splitted yarns (for textile layers), and complex shape of the structural stitching loops [1,2]. The variability includes also random nesting of layers, random overlap of "structural" and "non-structural" piercing patterns and openings (for NCFs), wide distribution of the opening dimensions, etc. [3].

As a result, the composite has a complex hierarchical (meso- and micro-) structure having numerous stress concentrations and significant randomization. The meso level (0.1–100 mm) includes the yarn loops (non-structural and structural), openings in the fibrous plies, gaps between the plies, etc. The micro level (10—100 μm) embraces the variable fibre content in a ply and yarn.

Investigation of such a composite is difficult due to a bulk of parameters like stitching method/speed, distance between stitches and seams, needle dimensions, properties of the preform/yarn,

yarn tension, etc. The interpretation of experimental data is thus sophisticated and case-dependent, and a broad experience is required for a generalized understanding.

As indicated by earlier studies [4–16], the distorted internal structure usually decreases (even slightly) the stiffness and strength under the in-plane tension or bending, although some improvements are occasionally observed if a small (less than 0.01 stitches/mm^2) stitch density is used. The modes I and II interlaminar fracture toughness are improved considerably, sometimes by a factor of 10 [8,9], that naturally happens for high stitch densities. Insufficient data exist for the through-the-thickness stiffness. It is also vital to clarify the failure mechanisms, especially under tension [11].

Earlier studies of progressive damage in NCFs [17–19], structurally stitched woven [20], and NCF composites [16,21] employ acoustic emission and X-ray to investigate the damage onset and development in different stages of the loading process. The present study uses similar techniques, described in detail in [22], and aims also at a comparison of the stiffness and damage responses according to the textile internal structure. The object of study is a typical carbon/epoxy composite based on an NCF preform, unstitched or structurally stitched with a carbon thread and different piercing steps. However as mentioned above, a "typical" stitched composite is a loose concept, and in reality it results rather in a case study.

2. Materials

0/90° and ±45° Saertex® NCFs having the areal weight of 556 and 540 g/m^2 respectively are used as the raw materials, Fig. 1.

---

* Corresponding author. Tel.: +32 16 32 13 00; fax: +32 16 32 19 90.
E-mail address: Stepan.Lomov@mtm.kuleuven.be (S.V. Lomov).
[1] Present address: Univ. of Twente, Faculty of Engng. Tech., Production Tech., The Netherlands.
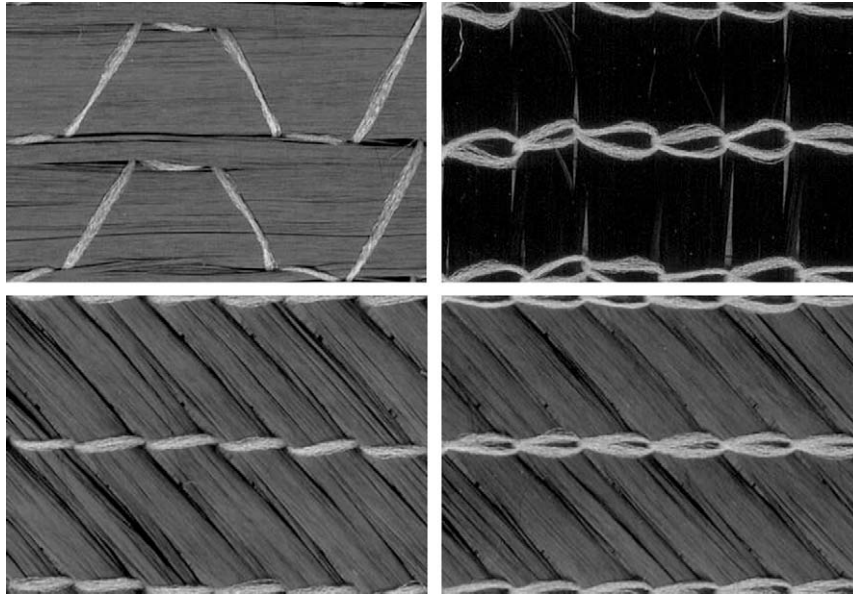[2] Present address: Composittrailer NV, Belgium.

Fig. 1. 0/90° (top) and ±45° NCFs (bottom). Left—face side, right—backside.

"0°" direction corresponds to the machine direction of production of NCF, or that of the non-structural stitching, i.e. to the horizontal direction in this figure. The areal weight of ±45° and 90° plies is 267 g/m^2, while 0° ply weights 283 g/m^2. The carbon fibre bundles are knit together with a thin thermoplastic yarn (7.4 tex, 2.6 × 5 mm tricot + chain knitting pattern, 6 g/m^2). The preform is composed of six layers in a symmetric stacking sequence [45/−45/0/90/45/−45]$_s$.

For the structural stitching, 1 K carbon rowing [23] and tufting method (KL RS 522 stitching head mounted on a KUKA-robot) are employed, with square piercing pattern 5 × 5, 7 × 7, or 9 × 9 mm. The machine direction coincides with 0° direction of the preform. The tufting was adjusted to produce about 4 mm high free loops at the backside. However, first 5 × 5 mm tufting resulted in only about 2 mm high backside loops, due to low friction of the carbon roving in the Rohacell foam that was used as the base plate. Because of this the loops were pulled out a bit when the needle was moved out. This preform is further denoted as "5 × 5 mm short loops" (a normal one was also produced). Typical photos of the stitched preform are shown in Fig. 2.

During the knitting and tufting, fibre-free zones (called "openings") appear; they are naturally oriented along the global fibre orientation in the ply. In order to characterize their on-surface geometry, the NCF and stitched preform surfaces are scanned with a resolution of 1200 dpi (21.1 μm/pixel). Then, about 100 dimensions are marked with lines in a separate image layer for each object type (length or width of the openings, yarn width). The layer is saved as a bitmap file and committed to a Matlab applet which searches for the marked lines and calculates their lengths. Finally, the average values and standard deviations are assessed, Table 1.

The face- and backsides of ±45° NCF naturally show very close values, due to a similar configuration of the knitting loops. In 0/90° fabric, the face side (0°) openings are much longer than the backside ones, obviously due to a 2.7 mm step in the machine direction which in this case coincides with the fibre (0°) direction.

In the structurally stitched preforms, the openings have about the same length but are naturally wider due to thicker yarn. Thus the length-to-width ratio is much lower than in an NCF. It can be related to a yarn tension in knitting and, therefore, larger compaction of the fibre tows during the non-structural stitching (which is in fact a knitting operation). Then a new "structural" opening cannot spread far sideways, since it is locked in the compacted zones between the non-structural stitching sites.

Composite plates (stitched and non-stitched) are produced by means of VAP (Vacuum Assisted Process) technology, using RTM-6 epoxy resin. The final thickness is 3.2–3.5 mm that gives the average fibre volume fraction (V_f) of 54% (without taking openings into account). Several pieces are inspected with an optical microscope for details of the internal structure. Measured dimensions are listed in Table 1, which reveals significant (about 30–50%) reduction in the size of the openings if compare with the dry preforms. This effect should be attributed to severe densification of the fibrous plies in the mould (thickness in the dry state is about 4.2 mm). Taking average rhomboid 6.0 × 0.75 mm ("structural") and 4.1 × 0.43 mm ("non-structural") openings, it can be estimated that local V_f in plies after the stitching is 70%, and the
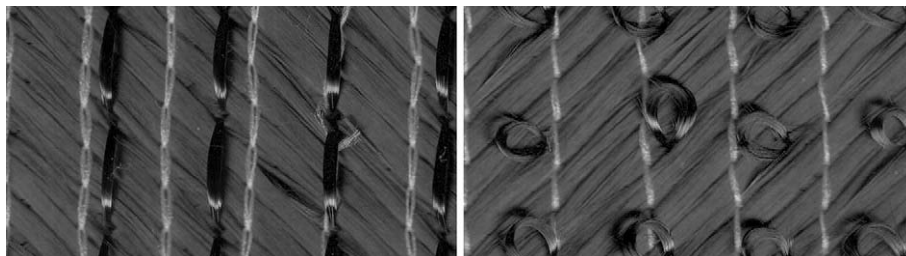

Fig. 2. Face side (left) and backside (right) of a 7 × 7 mm stitched preform.

Table 1
Measured dimensions of the "openings" and the stitching yarn. In the case of stitching, only the "structural" openings are measured.

	Length (mm)	Width (mm)	Length/width ratio	Stitching yarn width (mm)	Loop height (mm)	Loop width (mm)
Dry 0/90 NCF, face	7.3 ± 3.0	0.33 ± 0.09	22.2	–	–	–
Dry 0/90 NCF, back	3.4 ± 0.8	0.26 ± 0.04	13.2	–	–	–
Dry ±45 NCF, face	9.3 ± 3.5	0.50 ± 0.08	18.7	–	–	–
Dry ±45 NCF, back	9.2 ± 2.1	0.49 ± 0.06	18.8	–	–	–
Dry stitched preform, face[a]	9.9 ± 1.6	1.16 ± 0.15	8.6	0.86 ± 0.09	–	–
Dry stitched preform, back[a]	9.1 ± 2.4	1.10 ± 0.13	8.3	0.94 ± 0.21	3.4 ± 0.5	2.6 ± 0.3
Composite, unstitched	4.1 ± 0.9	0.43 ± 0.08	9.5	–	–	–
Composite, 5 × 5 short, face	6.0 ± 0.9	0.75 ± .15	8.0	1.36 ± .28	–	–
Composite, 5 × 5 short, back	6.4 ± 1.1	1.11 ± .28	5.8	0.64 ± .10	1.4 ± 0.2	1.8 ± 0.2

[a] Averaged for all stitching cases (except for the backside loop data for 5 × 5 short). Actually only the opening length shows some dependence on the stitching density; it varies from 7.9 mm (5 × 5 mm pattern) to 11.5 mm (9 × 9 mm one). Similar observation (opening width depends mainly on the needle thickness) is reported in [3].
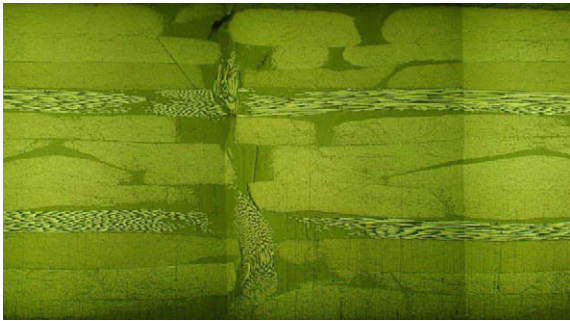

Fig. 3. Typical micrograph of a cross-section cut in 90° direction (across stitching).

openings occupy about 16% of the total volume. Similar is observed for a tufted woven preform having approximately the same original V_f [20].

Typical micrograph of a stitching site is shown in Fig. 3. Several cracks are seen here near the stitching yarn. This is probably due to shrink effects appearing along the complex yarn paths, where the mismatch of the thermal expansion coefficients takes place.

The material properties—Young's modulus, E, Poisson's ratio, v (theoretically estimated for the transversal direction), ultimate tensile stress, σ_{ult}, etc.—are listed in Table 2.

3. Experimental

Mainly uniaxial tensile tests are discussed in this paper; out-of-plane compression and 3PBT tests are done also but rather for a qualitative characterization.

The tensile tests are performed according to ASTM D3039; 250 mm long specimens having a constant $(3.2–3.5) \times 30$ mm cross-section and 60 mm long end tabs are used. Series of six (unstitched) or eight (stitched) specimens are tested for 0° (along the structural stitching) and 90° directions, at a 3 mm/min crosshead displacement rate. The tests are monitored with the acoustic emission (AE) and full-field strain registrations.

The latter one is used to register as local strain distributions, as well as to measure the average strains in the specimen (optical extensometer). All the strains and displacements used below are measured in this way. First, four specimens in a series (two for unstitched) are tested until failure. Here, since the AE sensors should be removed before the specimen failure, the loading is not completely monotonical but is paused at a certain load level. Two other specimens are tested until the "mass crack onset" strain level (ε_2 as explained in detail below, Section 3.4) which is registered with AE equipment on the previous specimens. Finally, two specimens are tested until "damage onset" level (ε_1). For all the strain levels (ε_1, ε_2, and ultimate) the specimens are further inspected with X-rays to reveal the damage development features.

3.1. Stiffness

Table 3 summarizes the measured Young's moduli and Poisson's ratios, averaged within a 30–110 MPa stress range. In all the cases 90° direction is slightly stiffer than 0° one, while the first assumption was opposite due to denser (by 6%) 0° ply in 0/90° NCF. For the Poisson's ratios there is the same trend: tension in 90° direction usually gives slightly larger mean values. Whilst almost inside the scatter intervals, some of the differences are statistically significant at a good confidence level.
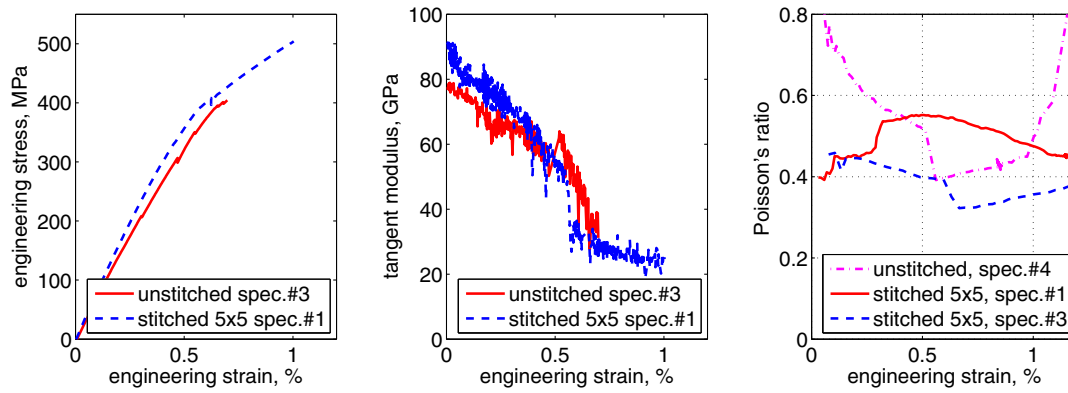
Table 2
Properties of the composite constituents (longitudinal/transversal).

	Material	Fibre ⌀ (μm)	Twist (t/m)	Density (g/cm³)	Linear density (tex)	E (GPa)	v	σ_{ult}^{tens} (MPa)
Ply	Tenax HTS 5631	7	0	1.77	0.068	240/25	0.270/0.028	4300/–
Ply	PES 76/24/1	2	Z24	1.38	74	2.7	0.30	72
Stitch	Tenax HTA 5241	7	S15	1.76	67	238/14	0.230/0.014	3950/–
Resin	HexFlow RTM6	–	–	1.14	–	2.89	0.38	75.0

Table 3
Stiffness properties, test data. The moduli are given in GPa. E_z and $v_{z,0}$ are measured under out-plane compression; other values—under in-plane tension. The levels of confidence (%) are given for the differences between 0° and 90° directions.

Stitching	E_0	E_{90}	LOC	E_z	$v_{0,90}$	$v_{90,0}$	LOC	$v_{z,0}$ ($v_{z,90}$)
n/a	39.3 ± 2.5	41.4 ± 1.6	84	15.6 ± 3.2	0.45 ± 0.08	0.56 ± 0.08	94	0.023 ± 0.012
9 × 9 mm	39.7 ± 2.6	41.1 ± 3.2	65	16.6 ± 4.9	0.43 ± 0.09	0.51 ± 0.17	90	0.051 ± 0.021
7 × 7 mm	39.4 ± 3.0	41.6 ± 2.7	86	19.1 ± 3.4	0.44 ± 0.13	0.54 ± 0.10	90	0.038 ± 0.022
5 × 5 mm	38.9 ± 1.7	40.1 ± 2.1	76	–	0.48 ± 0.07	0.53 ± 0.12	68	–
5 × 5 mm Short	38.1 ± 1.7	40.2 ± 2.0	96	14.5 ± 3.4	0.50 ± 0.12	0.48 ± 0.06	32	0.039 ± 0.015

Fig. 4. Typical load curves (left), tangent moduli (center), and Poisson's ratios (right) under uniaxial tension. Left and center – 0° loading, right – 90° loading.

Increased stitching density is not accompanied by increased stiffness in 0° direction. This is a reasonable result implied by a negligible amount (about 0.2%) of carbon fibres added to this direction when the stitching step changes from 5 to 9 mm. On the other hand, the stiffness does not decrease, despite the distorted fibre orientation (due to openings) which is probably compensated by an increased local V_f. The final conclusion is that the structural stitching has a minor effect on the in-plane stiffness in this case. This agrees with the most of earlier results for a wide range of structurally stitched materials reported in other studies [6,10,11], for a relatively high density of the stitching, comparable to the one studied here (0.01 stitches/mm^2 and more).

Fig. 4 shows typical load curves and variations of the tangent moduli during loading. First, the material exhibits a gradually decreasing (in about 40%) stiffness. This effect should mainly be explained by crack formation and non-linear matrix deformation.

At a transition strain of about 0.3–0.5%, a dramatic drop of the stiffness occurs within this narrow strain range. As shown below in Section 3.4, this strain range corresponds to the mass crack formation in the off-axis plies of the composite. Similar behaviour is observed for the Poisson's ratio, Fig. 4(right), which also shows a distinct change at this transition strain. It is also noticeable that the Poisson's ratio plots have a wide variation even in the same series; its reason is still not clear for the authors.

In the following region, the material response stabilizes and keeps almost constant until the final failure. This is obviously due to the fact that the stiffness is now dominated by tension of the fibres co-axial to the load. A small stiffness reduction can be caused by a non-linear deformation and continued cracking in the matrix.

3.2. Strength

Table 4 summarizes the measured ultimate strains and stresses. It is seen that the structural stitching increases the ultimate load; this is more prominent for denser stitching (5 × 5 mm) than for the spaced one (9 × 9 mm). This agrees with earlier observations for certain stitched composites [4,11], while for other configura-

tions the same studies report about degrading tensile strength with decreasing stitch spacing. Generally the present data are in the range of the summary results for stitched materials with different textile architecture, collected in [11] which show that, with few exceptions, stitching improves or degrades the tensile strength by less than 15–20%.

The increased strength should probably be attributed to a better interlaminar fracture toughness improved by stitching. This is suggested by the positive role of denser stitching. As demonstrated, for example, in [24], local delaminations, resulting from the out-of-plane and shear stresses caused by waviness of fibres in an NCF, can trigger fibre fracture and final failure of the sample. One can make a conjecture that in the present case also the delamination is either a controlling factor for strength or is closely interrelated with the tensile fracture. Increase of the through-the-thickness strength, provided by the stitching, can delay the local delaminations. Another reason can be that the local V_f and local stresses vary between different stitching cases, due to a varying number of openings per unit area and their different average length, Table 1.

Photos of the specimens are shown in Fig. 5 and depict that the stitching direction strongly affects the extension of delamination. While it considerably decreases under 90° loading (cross direction to the stitching), images after 0° loading show similar delaminated areas (slightly larger for the unstitched specimens).

Fig. 4(right) reveals a prominent increase of the Poisson's ratio in the unstitched specimen prior to its failure; no such growth is observed for the stitched ones. This can be due to extensive delamination in the unstitched composite, when outer ±45° layers lose bonding with inner 0/90° layers and then naturally become more compliant in tension.

3.3. Damage development: DIC

Fig. 6 shows typical strain fields in different specimens. It is seen that the tufting causes prominent strain concentrations at the stitching sites, although the backside, Fig. 6b, gives some blurred pattern, probably due to yarn loops. Analysis of the strain history in such local maximums often reveals almost constant

Table 4
Strength properties, test data (0/90°).

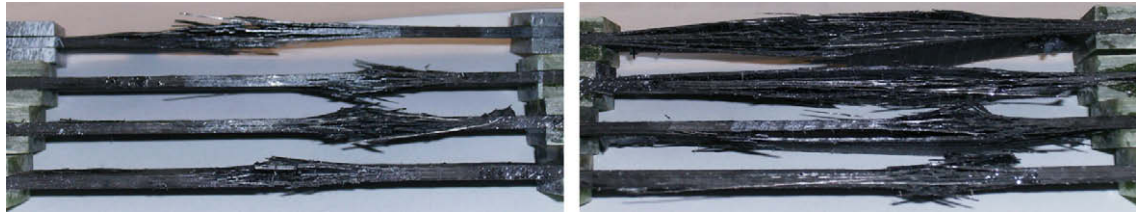| Stitching	ε_1 (%)	ε_2 (%)	ε^{ult} (%)	σ^{ult} (MPa)
n/a	0.16 ± 0.10/0.13 ± 0.10	0.57 ± 0.05/0.45 ± 0.09	1.17 ± 0.14/1.43 ± 0.04	432.6 ± 14.9/390.1 ± 0.7
9 × 9	0.11 ± 0.06/0.12 ± 0.08	0.39 ± 0.07/0.36 ± 0.06	1.42 ± 0.13/1.40 ± 0.09	472.7 ± 21.8/440.6 ± 25.3
7 × 7	0.08 ± 0.04/0.10 ± 0.05	0.31 ± 0.06/0.25 ± 0.02	1.41 ± 0.09/1.44 ± 0.08	493.0 ± 20.0/457.3 ± 12.9
5 × 5	0.12 ± 0.04/0.08 ± 0.04	0.26 ± 0.06/0.22 ± 0.06	1.51 ± 0.02/1.52 ± 0.04	493.1 ± 15.3/478.3 ± 6.5
5 × 5 Short	0.13 ± 0.04/0.11 ± 0.04	0.28 ± 0.04/0.27 ± 0.09	1.49 ± 0.07/1.49 ± 0.09	473.0 ± 5.7/478.1 ± 13.8

Fig. 5. Specimens failed under 0° (left) and 90° (right) loading. From top to bottom: unstitched, stitched 9 × 9, 7 × 7, and 5 × 5 mm.
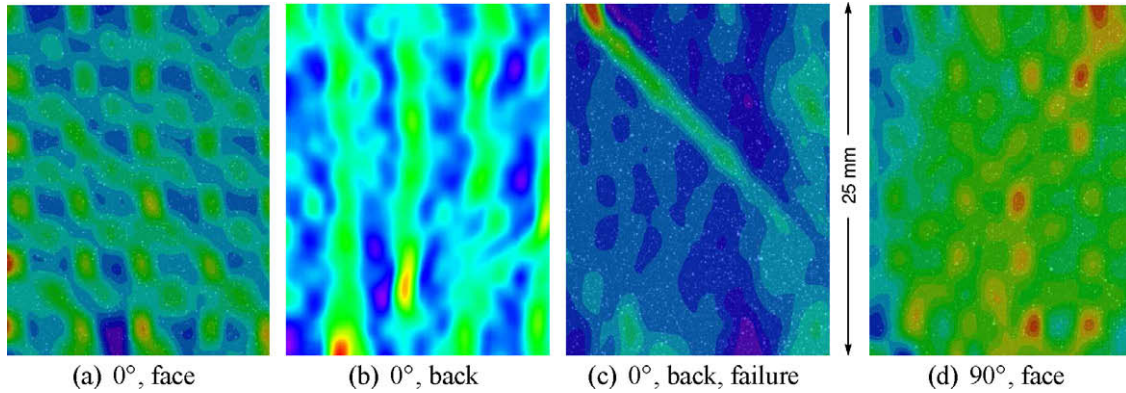

(a) 0°, face   (b) 0°, back   (c) 0°, back, failure   (d) 90°, face

Fig. 6. Typical surface strains ε_x under loading in 0° (a–c) and 90° (d) directions. The load is applied in horizontal direction; almost the whole specimen width (25 out of 30 mm) is shown. Cases (a, b, d) present 5 × 5 stitched specimens, case (c)—a 9 × 9 one.

strain rate until a moment, when it starts to increase rapidly, Fig. 7(left). This moment can be attributed to the gross failure onset; afterwards, the local strain more and more differs from the average one. For example, the specimen shown in Fig. 6a fails at the average strain of 1.5%, while the ultimate local strain approaches 3%; the rapid increase starts at about 1.35% of the average strain. Some plots in Fig. 7(left) show sudden jumps at lower average strains (0.6%, 0.9%) presumably indicating a stepwise fracture propagation.

However not all stitching sites show such a growth; the strain rate is often constant or even decreases when the specimen approaches the ultimate state. This suggests that the damage accumulates at selected (having unfavourable strength) stitching sites. It should be noted that only outer ±45° layers are available for optical measurements, and inner 0/90° layers may have other strain patterns and specifics of their variation under loading. Fig. 7(right) shows typical strain distributions across the specimen width. The profiles are taken here through the stitching sites which show again a strong strain concentration.

3.4. Damage development: AE

Fig. 8 shows examples of the cumulative energy of events and cumulative event count calculated using AE data. The damage onset is detected at low (about 0.05–0.15%) strains, when a few low-energy events occur with low frequency. The corresponding strain level is further denoted as ε_1 and may be attributed to growing shrink cracks (like observed in Fig. 3) or initiation of new cracks in the weakest locations (see Section 3.5). At a certain moment the frequency of AE events increases, both the energy content and event count rise quickly, and the specimens start to emit popping sounds indicating extensive appearance of relatively large cracks, presumably in the off-axis plies. This is called below as "mass crack formation"; the corresponding strain level is further denoted as ε_2.
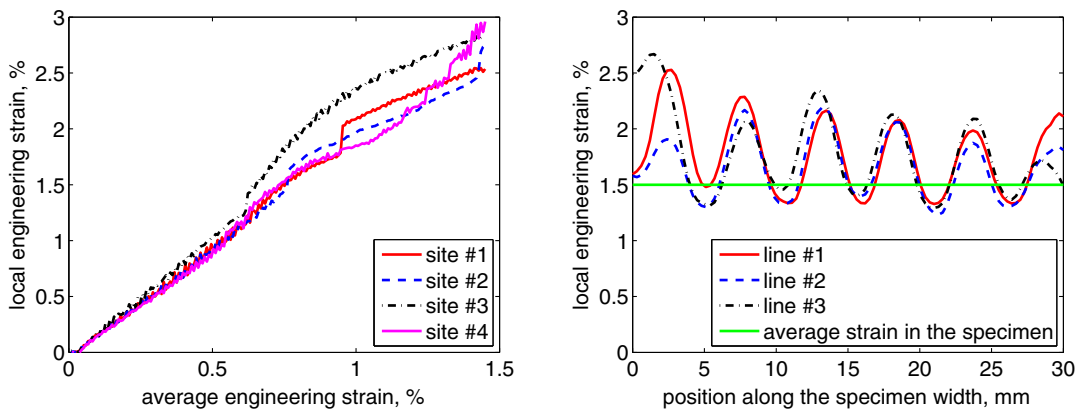

Fig. 7. Typical maximal (at stitching sites) ε_x strain growth vs. applied average strain (left) and distributions of ε_x strains across the specimen width at failure moment (right).
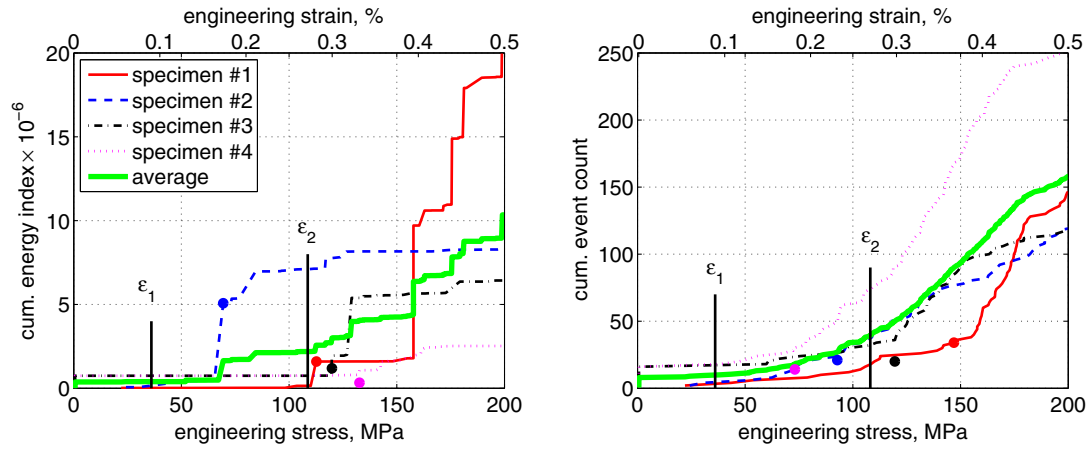
Fig. 8. Definition of the average characteristic strains ε_1 and ε_2 using AE data for conventional crack energy (left) or number of events (right). 5×5 mm tufted specimens, $0°$ loading. Values of ε_2 for different specimens are marked with filled dots.

The influence of stitching is depicted by Fig. 9. It is seen that the tufted specimens show larger energy index and event count under a moderate load. Under higher loads the ratio changes, and both criteria indicate lower damage in the tufted specimens. This is revealed very well by the cumulative sum of AE event counts, Fig. 9(bottom). It is also interesting to note that the event curves have two almost linear parts for the unstitched specimens; this means that the increase of the event number is almost constant within each part. The same is observed for a woven fabric studied in [20].

Averaged ε_1 and ε_2 strains are shown in Table 4. The listed values of ε_2 are determined using AE event count plots. If AE energy plots are used, ε_2 is in 30–70% higher and shows wider variations. This presumably indicates a natural scenario when numerous small cracks appear first, and then a portion of them starts to grow with a higher fracture energy. It is seen also that increased stitching density results in decreased ε_2, i.e. the damage onset occurs earlier, but as noted above the final (failure) damage is lower. The influence on ε_1 is obscure due to similar mean values and wide variations.
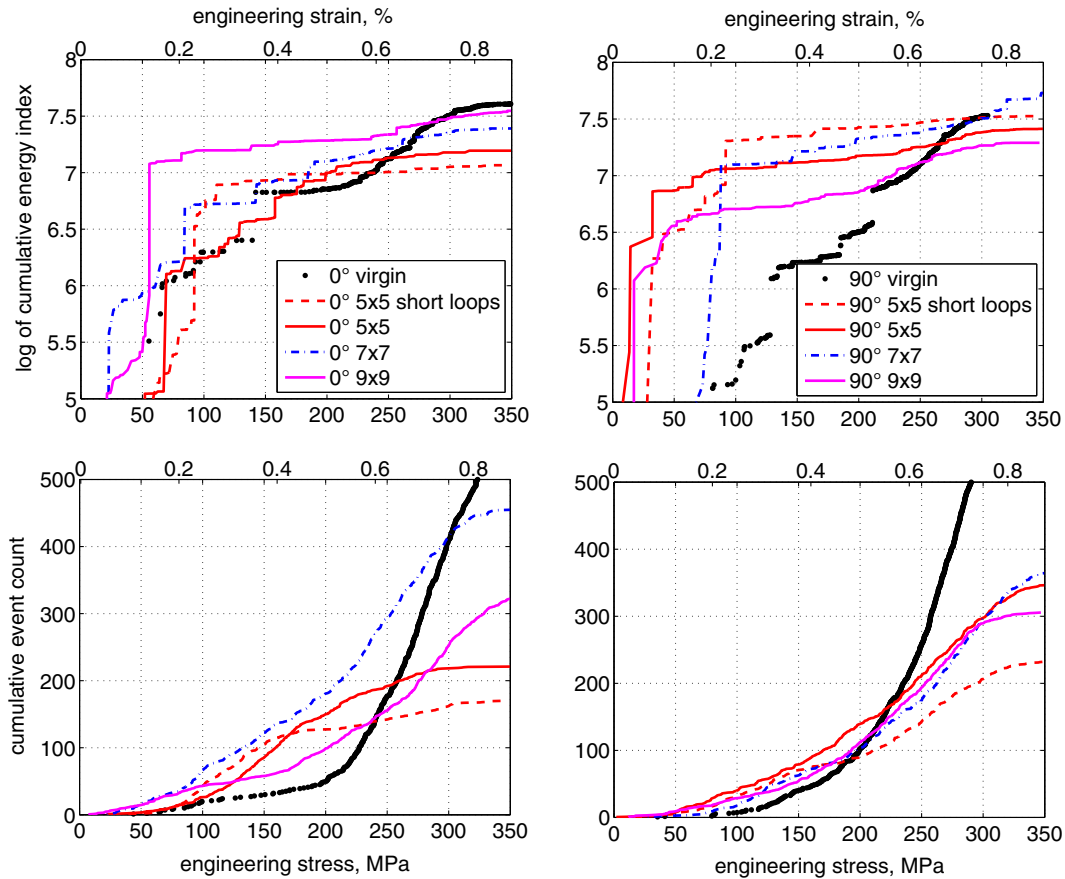

Fig. 9. AE energy in logarithmic scale (top) and cumulative sum of AE event counts (bottom). Averaged in each series for $0°$ (left) and $90°$ (right) loaded specimens.
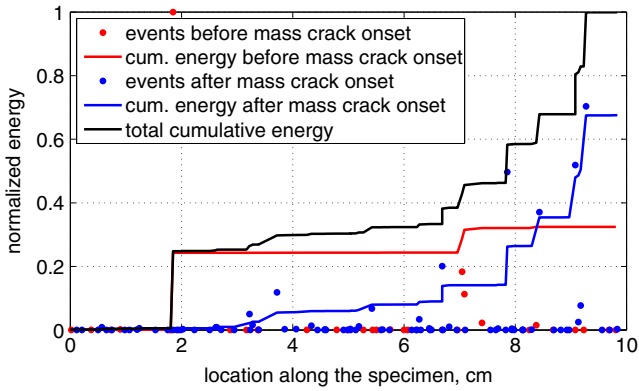
Fig. 10. Location of crack events, using AE data. 5×5 mm tufted specimen # 1, 0° loading. The cumulation is performed along the specimen (between AE sensors).

Fig. 10 shows the registered positions of events along the specimen length. The high-energy events are distributed with intervals which are close to the stitching length (5 mm in the present case). Therefore it can be suggested that these cracks appear at the stitching sites. If plotted in the logarithmic scale, the low-energy events are distributed quite evenly; this suggests that the most of them are caused by the non-structural stitching which has different positions in each layer, due to a random shift in the lay-up.

3.5. Damage development: X-rays

Fig. 11 shows typical X-ray images taken for unstitched and stitched specimens wetted in a special penetrant. The images reveal clearly that the cracks appear near the stitching sites; this occurs even due to the non-structural stitching, while the tufting provokes to yet larger clusters of cracks. The clusters are mainly confined in the plies oriented in ±45° to the loading direction, although relatively rare cracks appear in 0/90° plies also. This material degradation mechanism is in contrast with the first assumption that the cracks should first appear in the plies transversely oriented to the load direction.

It is seen also that the non-stitched composite, Fig. 11(left), does not show such almost continuous cracks as it occurs in the structurally stitched one, Fig. 11(right). In the former case, under almost the same load, the cracks are much shorter despite equal length of the resin-rich "openings", Table 1. This suggests that the width of openings (which is much larger for the "structural" openings) has the primary impact on the crack growth.

Fig. 11(middle) depicts that large cracks appear already at about ε_2 strain level but not in all stitching sites (this is also observed above in Section 3.3 when analyzing the full-field strain data). Higher load provokes for cracks at every site, and these cracks form a quadric damage pattern, Fig. 11(right).

3.6. Out-of-plane compression

Specimens having a 20×20 mm in-plane size are compressed between two steel plates at a cross-head displacement rate of 1 mm/min. Series of five specimens are tested. The measured Young's modulus, E_z, and Poisson's ratio, $v_{z,0}$, are summarized in Table 3. The stitching is seen to somehow stiffen the material, on the margin of a statistical significance; 5×5 mm case is exceptional and could be due some error in the test procedure.
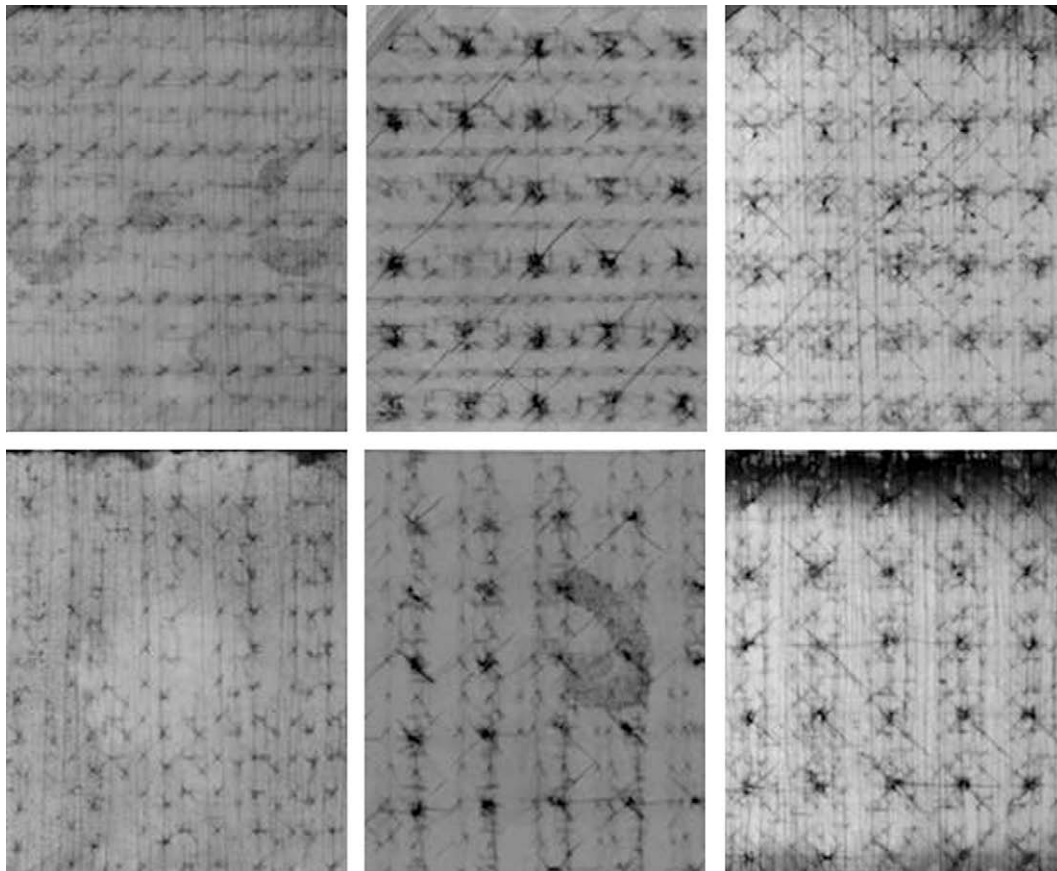

Fig. 11. X-rays for unstitched (left) and 5×5 mm tufted (middle and right) specimens loaded respectively until 1.0%, 0.2%, or 1.15% average strain in 0° (top) and 90° (bottom) directions. Whole specimen width is shown (vertical dimension in the images).
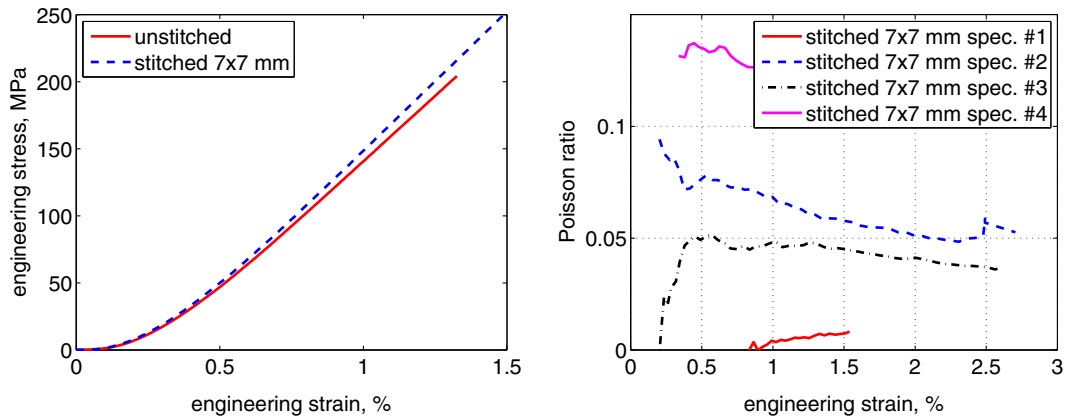
Fig. 12. Typical progression of the load curves (left) and Poisson's ratios (right) under uniaxial out-of-plane compression.

The load curves are quite linear except for a relatively narrow initial range, Fig. 12(left), when the stiffness is reduced, probably due to some wavy surface of the composite resulting in a variable contact area. A possible non-parallelism of the loading plates can also cause the non-linearity but this should not be prominent here, since the specimens are quite small. The overall response is linear even at the end of the tests, when the engineering strain reaches 2–3% and thus non-linear effects in the matrix could be expected.

Typical variations of the Poisson's ratio during the loading are presented in Fig. 12(right); the plots depict a wide variation even in the same series; due to this reason, the Poisson's ratios listed in Table 3 are averaged within 1–2% strain range. The ratios cannot of course be obtained correctly in this test, because of friction between the specimen and loading plates; this should be an important factor for such a small thickness-to-width ratio.

Fig. 13 shows a typical strain field observed under compression. It is seen that significant strain gradients occur, obviously due to as the surface waviness mentioned above as well as a non-uniform internal structure. This starts already at the early loading stages and may be the reason for a relatively large distribution of the measured elastic properties, Table 3; although the strains are averaged over the whole area of interest shown in color in the figure, the gradients can produce some deviations of the mean values. This means also that the inelastic deformations do exist in the specimens but on the local level only, and are not prominent in the global response.

The wavy surface may also affect the standard deviation in another way, since some stitches can be situated at the cavities and thus resist the load in a different regime than the ones placed at the bosses. All this suggests that better test could be done either
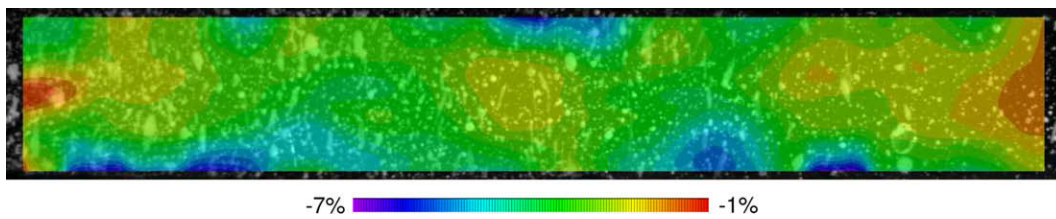

Fig. 13. Surface engineering strain ϵ_z under loading in z-direction (vertical one in the image). 5×5 mm stitched specimen, with short loops. The average ϵ_z strain level is −3.6%. Full specimen length (20 mm) and thickness (≈ 3.3 mm) are shown.
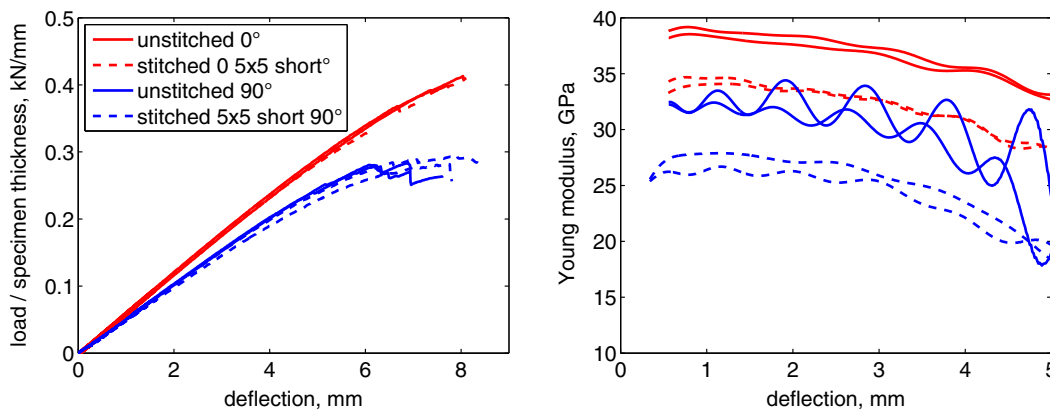

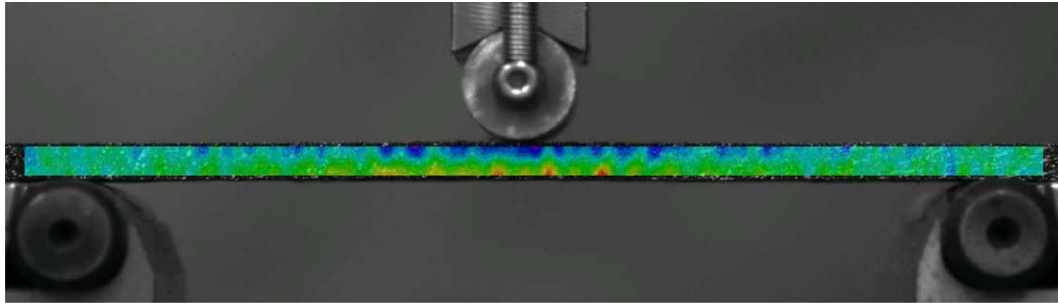**Fig. 14.** Load–displacement response (left) and flexural modulus (right) under 3PBT.

Fig. 15. Surface engineering strain ϵ_x under 3PBT (x is the horizontal direction in the image). Shown as in the undeformed state. 5×5 mm stitched specimen, with short loops.

by using larger series of specimens or by polishing their surfaces prior to the tests.

3.7. 3-Point bending

To characterize qualitatively the flexural behaviour, 3-point bending tests are performed on rectangular 125 mm long and 20 mm wide specimens having a 80 mm span length L, at a 2 mm/min displacement rate. The load nose and support pins diameter is 10 mm. Fig. 14 shows typical load curves and apparent (tangent) flexural moduli. The latter are estimated as

$$E = \frac{L^3}{4Wh^3} \frac{\Delta P}{\Delta \delta}, \qquad (1)$$

where W—width, h—thickness, δ—central deflection, P—applied load. This naturally gives lower values than listed in Table 3, since assumes geometrically linear bending and no shear (the latter should be insignificant for a large span-to-thickness ratio used here).

As seen in Fig. 14(right), the stitched specimens are prominently more compliant than the unstitched ones. This behaviour disagrees with the tensile tests (Table 3), where changes in the Young's modulus after the stitching are statistically insignificant. The reduced compliance is fairly reproducible; however, the authors do not have an explanation for this phenomenon.

A prominent difference between 0° and 90° directions can partially be explained by the fact that in the former case the stitching yarns are placed along the bending profile thus stiffering the response (this plays a larger role here than in tension); another (probably the primary) reason is thicker 0° plies in the NCF.

The ultimate strength is most likely improved but this is not clear due to a limited number of specimens (only two in each series). It is observed that the unstitched specimens fail by a combination of wide ply delamination, kink (at concave side) and tensile (at convex side) fibre damage. In the stitched specimens the latter ones appear also but the inter-ply debonding is less pronounced and is confined near the load nose.

A typical strain field is shown in Fig. 15. The edge of this specimen passes the stitching sites, which cause prominent strain gradients, especially close to the bottom surface.

4. Conclusions

This paper deals with an experimental characterization of structurally stitched NCF laminates, vs. the unstitched one. The main results are

- The structural stitching produces numerous fibre-free zones ("openings") in a stitched preform, which can occupy a large amount of its surface. In the present study, the surfaces of an NCF fabric contain about 15% of "openings"; tufted preform—about 30%; compression in the mould reduces them to 7% and 9%, respectively. Thus, while the average V_f is not much increased by the structural stitching, the local one increases by about 16% (taking both "structural" and "non-structural" openings and assuming an uniform fibre compaction between them).
- The structural stitching yarns and "openings" produce a negligible influence on the in-plane components of the homogenized stiffness matrix; this observation corresponds to the most of earlier results obtained by other authors [6,10,11]. The out-of-plane stiffness is improved by about 15%.
- The stitching considerably reduces the inter-ply delamination and amount of damage. The ultimate tensile load increases; this is more noticeably for a denser stitching than for a spaced one. This tendency agrees with some earlier studies [4,11] and may be produced by a better interlaminar fracture toughness, which is probably a controlling factor for the ultimate strength of this particular composite configuration.
- The stitching sites can play a role of stress concentrators and trigger damage (higher stitching density results in earlier damage onset) but the general effect can be positive. For example in the present case, the acoustic emission reveals that the tufted specimens show larger crack energy index and event count under a moderate load than the unstitched specimens. On the contrary, under higher loads both criteria indicate lower crack development in the tufted specimens.
- The structural stitching improves also the delamination resistance under 3-point bending; this agrees with other studies for mode II loading, e.g. [9]. The bending stiffness is decreased.
- It can be concluded that for the studied material configuration the structural stitching is a favourable factor. The literature review shows, however, that it can be not the case for other configurations, which sometimes give e.g. a significant tensile strength reduction after stitching [10,12], or degrading tensile strength with decreasing stitch spacing [4,11], or larger damage intensity in a tufted material at high strains [16]. Therefore this article shows rather a case study in respect with the quantitative results, although some qualitative ones (improved interlaminar fracture toughness, strain accumulation at the stitching sites, etc.) are innate for the stitched composites in general.

Materials Engineering, K.U. Leuven) for assistance with the mechanical testing and polishing equipment.

References

[1] Lomov SV et al. Carbon composites based on multiaxial multiply stitched preforms part 1. Geometry of the preform. Composites: Part A 2002;33:1171–83.

[2] Koissin V et al. Internal structure of structurally stitched NCF preform. In: Proceedings of 12th European conference on composite materials (ECCM-12), Biarritz, France; August 29–September 1, 2006 [CD-edition].

[3] Koissin V et al. On-surface fiber-free zones and irregularity of piercing pattern in structurally stitched NCF preforms. Adv Compos Lett 2006;15(3):87–94.

[4] Kang TJ, Lee SH. Effect of stitching on the mechanical and impact properties of woven laminate composite. Composites: Part A 1994;28(16):1574–87.

[5] Larsson F. Damage tolerance of a stitched carbon–epoxy composites. Composites: Part A 1997;28:923–34.

[6] Mouritz AP, Leong KH, Herszberg I. A review of the effect of stitching on the in-plane mechanical properties of fibre-reinforced polymer composites. Composites: Part A 1997;28:979–91.

[7] Cox BN, Flanagan G. Handbook of analytical methods for textile composites. NASA report; 1997.

[8] Dransfield KA, Jain LK, Mai YW. On the effects of stitching in CFRPs-I: model I delamination toughness. Compos Sci Technol 1998;58:815–27.

[9] Jain LK, Dransfield KA, Mai YW. On the effects of stitching in CFRPs-II: mode II delamination toughness. Compos Sci Technol 1998;58:829–37.

[10] Mouritz AP et al. Review of applications for advanced three-dimensional fibre textile composites. Composites: Part A 1999;30:1445–61.

[11] Mouritz AP, Cox BN. A mechanistic approach to the properties of stitched laminates. Composites: Part A 2000;31:1–27.

[12] Beier U et al. Mechanical performance of carbon fibre-reinforced composites based on stitched preforms. Composites: Part A 2007;38:1655–63.

[13] Han XP et al. Experimental study on the stitching reinforcement of composite laminates with a circular hole. Compos Sci Technol 2008;68(7–8):1649–53.

[14] Nie J et al. Effect of stitch spacing on mechanical properties of carbon/silicon carbide composites. Compos Sci Technol 2008;68(12):2425–32.

[15] Yoshimura A et al. Improvement on out-of-plane impact resistance of CFRP laminates due to through-the-thickness stitching. Composites: Part A 2008;39(9):1370–9.

[16] Colin de Verdiere M et al. Evaluation of the mechanical and damage behaviour of tufted non crimped fabric composites using full field measurements. Compos Sci Technol 2009;69(2):131–8.

[17] Truong Chi T et al. Carbon composites based on multiaxial multiply preforms. Part 4. Mechanical properties of composites and damage observation. Composites: Part A 2005;36:1207–21.

[18] Truong Chi T et al. Carbon composites based on multiaxial multiply stitched preforms. Part 7. Mechanical properties and damage observations in composite with sheared reinforcement. Composites: Part A 2008;39: 1380–93.

[19] Mikhaluk DS et al. Experimental observations and finite element modelling of damage and fracture in carbon/epoxy non-crimp fabric composites. Eng Fract Mech 2008;75(9):2751–66.

[20] Koissin V et al. Structurally stitched woven preforms: experimental characterization, geometrical modelling, and FE analysis. Plast Rubber Compos: Macromol Eng 2009;38(2–4):98–105 [ECCM 13 special issue].

[21] Heß H, Roth YC, Himmel N. Elastic constants estimation of stitched NCF CFRP laminates based on a finite element unit-cell model. Compos Sci Technol 2007;67(6):1081–95.

[22] Lomov SV et al. Experimental methodology of study of damage initiation and development in textile composites in uniaxial tensile test. Compos Sci Technol 2008;68:2340–9.

[23] Delivery programme and characteristics for Tenax filament yarn. Toho Tenax Europe GmbH, Germany. [www.tohotenax-eu.com]

[24] Mattsson D, Joffe R, Varna J. Damage in NCF composites under tension: effect of layer stacking sequence. Eng Fract Mech 2008;75(9):2666–82.